Soft Matter

Ice modulatory effect of the polysaccharide FucoPol in directional freezing

Journal:	*Soft Matter*
Manuscript ID	SM-ART-08-2023-001154.R1
Article Type:	Paper
Date Submitted by the Author:	17-Oct-2023
Complete List of Authors:	Guerreiro, Bruno; Universidade Nova de Lisboa Faculdade de Ciências e Tecnologia, UCIBIO-REQUIMTE, Chemistry Department Lou, Leo; University of California Berkeley, Rubinsky, Boris; University of California Berkeley College of Engineering, Department of Mechanical Engineering; University of California Berkeley College of Engineering, Department of Mechanical Engineering Freitas, Filomena; NOVA School of Science and Technology, Chemistry Department

ARTICLE

Ice modulatory effect of the polysaccharide FucoPol in directional freezing

Received 00th August 2023,
Accepted 00th January 20xx

DOI: 10.1039/x0xx00000x

Bruno M. Guerreiro[a,b], Leo T. Lou[c], Boris Rubinsky[c]†, Filomena Freitas[a,b]†

Directional freezing harnesses crystal growth development to create aligned solid structures or etchable patterns, useful for directed ice growth in cryobiology and cryoprinting for tissue engineering. We have delved into the ice-modulating properties of FucoPol, a fucose-rich, bio-based polysaccharide. Previous research on FucoPol revealed its non-colligative hysteresis in kinetic freezing point, reduced crystal dimensions and cryoprotective effect. Here, FucoPol reshaped developing sharp, anisotropic obloid ice dendrites into linearly-aligned, thin, isotropic spicules or tubules (cooling rate-dependent morphology). The effect was enhanced by increased concentration and decreased cooling rate, but major reshaping was observed with 5 µM and below. These structures boasted remarkable enhancements: uniform alignment (3-fold), tip symmetry (5.9-fold) and reduced thickness (5.3-fold). The ice-modulating capability of FucoPol resembles the Gibbs-Thomson effect of antifreeze proteins, in particular the ice reshaping profiles of type I antifreeze proteins and rattlesnake venom lectins, evidenced by a 52.6±2.2º contact angle (θ) and spicular structure generation. The high viscosity of FucoPol solutions, notably higher than that of sucrose, plays a crucial role. This viscosity dynamically intensifies during directional freezing, leading to a diffusion-limited impediment that influences dendritic formation. Essentially, the ice-modulating prowess of FucoPol not only reinforces its established cryoprotective qualities but also hints at its potential utility in applications that harness advantageous ice growth for intentional structuring. For instance, its potential in cryobioprinting is noteworthy, offering an economical, biodegradable resource, of easy removal, sidestepping the need for toxic reagents. Moreover, FucoPol fine-tunes resulting ice structures, enabling the ice-etching of biologically relevant patterns within biocompatible matrices for advanced tissue engineering endeavors.

1. Introduction

Ice crystal growth is the main predictor of cellular lethality during the freezing of biological samples[1]. To alleviate or fully suppress the mechanical damage cells undergo during crystallization, chemical additives are supplemented. These cryoprotectants are chemically very diverse, and usually categorized as small-molecule (*e.g.* glycerol, DMSO)[2] or polymeric agents (*e.g.* PVA[3], antifreeze proteins[4], polyampholytes[5–7], bio-based polysaccharides[2,8–11]). The several mechanisms of action previously ascribed to cryoprotectant molecules range from influences on solution viscosity[12], cell membrane properties, their direct interference on phase-change thermodynamics[13] and dynamic ice modulation. The latter can be studied by directional freezing *(start of revision block)*, a subtype of directional solidification using water as substrate, in which the development of a solid phase grows constrained to one direction in space (*i.e. Z*-axis). Under a thermal gradient, temperature fluctuations in the moving ice front will generate dynamic instabilities that eventually lead to ice dendrites[14–16]. While commonly employed in materials science[17], this technique has shown benefits in cryobiology[18,19]. Directionally frozen cells have shown higher post-thaw viability, reduced post-thaw culturing time and implementation into microfluidic devices[20]. In larger scale, the control of ice growth directionality, along with vitrification, have been highlighted as the best strategies for biological preservation of tissues and organs[21].

This study draws from the underlying concepts of crystal growth thoroughly described by Kurz and Fisher[22]. Fundamentally, the freezing rate applied controls ice front velocity and ice dendrite morphology[23], and consequent cell survival[24]. However, any perturbation in the original shape of the dendritic profile is a manifestation of dissolved solutes[25–28], which may diffuse into the bulk ice or remain rejected from the solid fraction and supersaturate at the interface[15,29]. Molecular interactions with the dendritic interface may generate ice shaping effects if there is a strong binding affinity, which will depend on molecular nature[2], molality and global charge. Such is the case of antifreeze proteins, which adsorb to particular facets of the ice front by an adsorption-inhibition mechanism[30], which inhibits ice growth on characteristic ice-binding regions, leading to dendritic profiles with recognizable patterns[31].

[a] UCIBIO – Applied Molecular Biosciences Unit, Department of Chemistry, School of Science and Technology, NOVA University Lisbon, Caparica, Portugal
[b] Associate Laboratory i4HB - Institute for Health and Bioeconomy, School of Science and Technology, NOVA University Lisbon, Caparica, Portugal
[c] Department of Mechanical Engineering, University of California at Berkeley, Berkeley, CA, USA
† Corresponding authors: rubinsky@berkeley.edu; a4406@fct.unl.pt
Electronic Supplementary Information (ESI) available: complete directional freezing setup schematics (Figure SI.1), FucoPol proof-of-concept 3D-printability (Table SI.1, Figure SI.2). See DOI: 10.1039/x0xx00000x

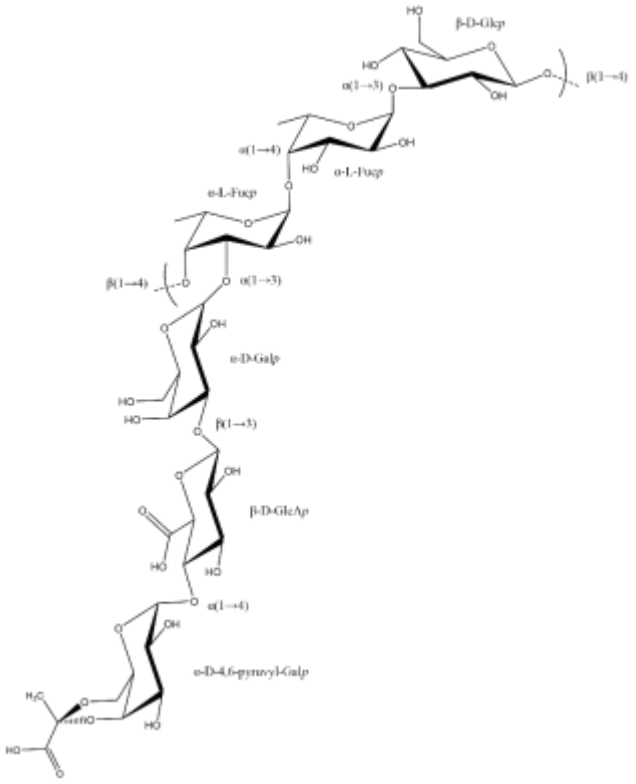

Figure 1. Structural repeating unit of FucoPol, a high-molecular-weight (1.7−5.8×10^6 Da) fucose-containing cryoprotective EPS produced by Gram-negative *Enterobacter* A47 (DSM 23139)[32]. FucoPol has a fucose, galactose, glucose, and glucuronic acid hexamer motif (2.0:1.9:0.9:0.5 M ratio), a main chain composed of a →4)-α-L-Fuc*p*-(1→4)-α-L-Fuc*p*-(1→3)-β-D-Glc*p*(1→ trimer repeating unit, and a trimer branch α-D-4,6-pyruvyl-Gal*p*-(1→4)-β-D-GlcA*p*-(1→3)-α-D-Gal*p*(1→ in the C-3 of the first fucose[8]. It also contains 13−14 wt.% pyruvyl, 3−5 wt.% acetyl, and 2−3 wt.% succinyl in its composition (not shown)[32]. The presence of glucuronic acid as well as the acyl substituents pyruvyl and succinyl confer a polyanionic character to the biopolymer[32].

The thermodynamic manifestation of this adsorptive binding at the microscale is known as the Gibbs-Thomson effect[33]. Thus, ice modulation properties can be probed by characteristic changes in dendritic shape, and attributed to classes of molecules with particular traits, such as molecular weight, structural conformation, solution viscosity and polyelectrolyte character *(end of revision block)*.

In this work, we explored the ice modulatory capabilities of FucoPol, a bacterial cryoprotectant biopolymer (**Figure 1**), in a directional freezing setup. The cryoprotective potential of FucoPol has been widely explored. First, the polymer acts as a crystallization initiator, successfully cryopreserving several animal cell lines by promoting earlier ice nucleation at sub-zero temperatures, significantly altering the kinetic freezing point of aqueous solutions, but reducing ice crystal dimensions to innocuous sizes[8]. Its performance was shown to be highly independent of solute composition, thus presenting great chemical flexibility in cryoprotective formulation development[9]. Second, it has a rheological shear-thinning behavior[34] reflective of a linearly-disposed chain, highly repeated, showing strong analogy to antifreeze proteins[35], and viscoelastic properties comparable to those of guar gum and fucogel[34]. Third, it distinguishes itself from common-use CPAs by its bio-based non-cytotoxic nature[8], very low osmolality and osmotic regulation effects due to its extracellular location and suspected cell membrane stabilization effects[36]. Lastly, we have recently shown that FucoPol can also influence the nucleation phase of metastable water, stabilizing its supercooled state in an exponential timescale and reducing the stochastic nature of nucleation events down to a narrower, predictable temperature interval[10]. All these properties reflect the acute interest in studying the influence of carbohydrate polymers in supercooled water systems, which is also a key aspect of directional freezing under a constant temperature gradient.

Here, we have determined the resulting ice dendrite morphology during directional freezing, for sucrose and FucoPol solutions, under two different cooling rates, and assessed features such as granularity, orthogonal striation, lamellar stacking and side branching. We performed photomicrographic geometric analysis of the resulting dendrites, as a means of quantifying practical performance indicators of growth modulation, such as lamellar thickness, tip protuberance, tilt angle, primary spacing, sharpness coefficients and growth anisotropy along the *Z*-axis. We hereby show that the cryoprotective polysaccharide FucoPol can also finetune dendrite growth morphology by yielding symmetric, linearly aligned tubular patterns of adjustable sharpness, with future impact in tissue engineering strategies.

2. Experimental Section

2.1 FucoPol production

FucoPol was produced by cultivation of *Enterobacter* A47 (DSM 23139) in a 2 L bioreactor (BioStat B-plus, Sartorius, Göttingen, Germany) under a fed-batch mode, using 40 g/L glycerol (Sigma-Aldrich, Germany) as the carbon source, according to the procedure previously described[37]. Briefly, FucoPol was extracted from the cultivation broth by dia/ultrafiltration, and characterized in terms of sugar monomers and acyl group compositions, and molecular mass distribution. The sample had number (M_n) and weight average molecular (M_w) weights of 1.9×10^6 Da and 3.3×10^6 (±0.3×10^6 Da), respectively, with a polydispersity of 1.70.

2.2 Sample preparation

Aqueous solutions of FucoPol were prepared at concentrations of 0.125, 0.25 and 0.5 wt.% (molar equivalent 1.25, 2.5 and 5 μM), and sucrose at 5 mM, using deionized water (type II, SKU S25293) as solvent. Dissolution was performed at room-temperature with a magnetic stir bar under slow agitation, for at least 30 minutes. Dissolution was considered complete when the solution had a homogeneous beige appearance.

2.3 Directional freezing stage design

A directional freezing stage was built for the real-time monitoring and image acquisition of growing ice dendrites, based on previous conceptual work[14,38]. The centerpiece is composed of a microscope glass slide with a 3D-printed

Bridgeman shape glued on top, to provide a bottom-sealed container for the aqueous solutions, and a 3 mm cotton cord at the leftmost edge of the rectangular shape. The Bridgeman shape, when displaced at constant velocity under a fixed temperature gradient, provides a constant cooling rate for crystal dendrite growth along an arbitrary *Z*-axis (**Figure 2**). The initial narrow region was intentionally designed to accommodate multidirectional ice growth arising from stochastic nucleation, resulting in confined crystals constrained by grain boundaries (**Figure 2**, *left panel*). Further progression of the interface towards the broad region of the Bridgeman shape promotes unidirectional growth of characteristic ice dendrites (**Figure 2**, *right panel*), whose morphological changes are very sensitive to the type of solute present, molality, viscosity, diffusivity, dendrite-water partition coefficient, thermal gradient and interface velocity. The centerpiece was placed on top of two temperature gradient blocks (one on each side) with a 5 mm gap designed to enable the microscope lens to visualize the center frame of the Bridgeman shape. The temperature gradient blocks were composed of three layers. From bottom to top: (i) a water-cooling block that contains inlet and outlet tubes in physical contact with water containers at –10 ℃ and 20 ℃, (ii) two Peltier modules initially calibrated at –5ºC and 4ºC, respectively, coupled to a temperature controlling device and (iii) a copper plate to enhance thermal conductivity and minimize thermal lag.

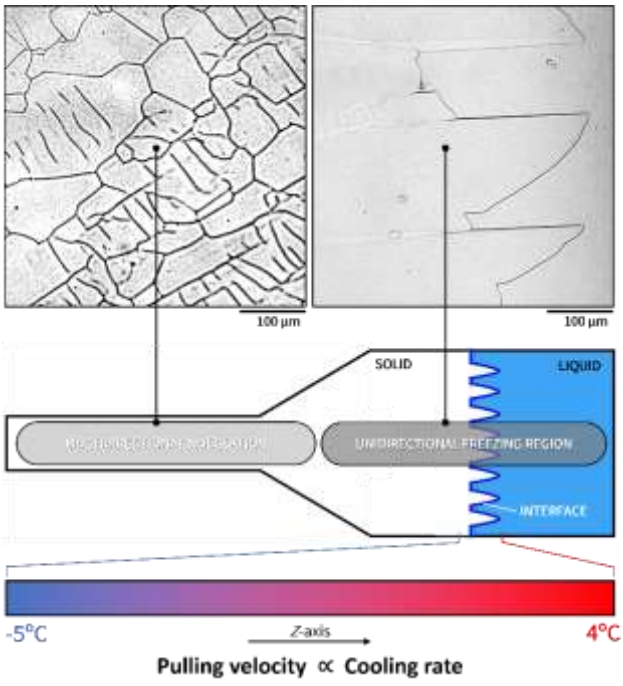

Figure 2. Schematics of the directional freezing of pure water for the setup used in this study. A Bridgeman shape, composed of narrow and broad regions, is displaced along a temperature gradient of 1.8º/mm. Initially, nucleation in the narrow region promotes multidirectional ice growth with grain boundaries. As the freezing temperature reaches the broad geometry of the Bridgeman sample holder, ice dendrites grow unidirectionally along the Z-axis, thus enabling directional freezing. Within thermal boundaries T_c and T_h of -5 and 4 ℃, respectively, the heat transfer gradient is linear, such that the cooling rate is constant and proportional to the applied mechanical pull. Cooling rates of 3.4 ℃/min (depicted) and 0.5 ℃/min were studied.

Prior to solution injection, the slide was cleaned with a compressed air duster and placed on the hot stage for 3 min to eliminate condensation before each run. Then, 1.5 ml of test solution was uniformly pipetted onto the Bridgeman shape and held for 5 min for thermal equilibration. Lastly, the syringe pump was activated to drag the slide and image acquisition was performed in the center frame. Image and video acquisition was performed by connecting a NIKON camera to the ocular lenses of a NIKON ECLIPSE microscope (100× amplification) and capturing the dendritic profile when it achieved a static frame of reference. Temperature sensing was performed with a K-type thermocouple in physical contact with the edge of each Peltier module. Pulling velocity was tuned with a conventional World Precision Instruments syringe pump. For establishing 0.5℃/min and 3.4℃/min cooling rates, pulling velocities of 58 µm/s and 400 µm/s were used, respectively. For a 5 mm gap between both Peltier plates, the effective thermal gradient was 1.8℃/mm.

2.4 Determination of contact angle and thermal hysteresis

The contact angle (θ) formed between the kink site of polysaccharide adsorption to the ice front, established as a geometrical plane orthogonal to ice growth and the ice-water interface (**Figure 4*g***) and dendrite width (*d*) were measured in triplicate for N=6 dendrites using the ImageJ software. Then, thermal hysteresis was calculated using the Gibbs-Thomson equation[39], which relates the ice-liquid interface curvature and an ensuing freezing point change to geometric limitations:

$$TH = \frac{4\gamma v^l T_f \cos\theta}{dL_f} \quad (1)$$

where T_f (273.15 K) is the equilibrium freezing point of unconfined pure water, v^l (1.091×10^{-3} m^3/kg) is the specific volume of ice at the given T_f, L_f (3.337×10^5 J/kg) is the specific latent heat of fusion of pure water at the given T_f, γ (30 mJ/m^2) is the ice−water interfacial tension, cos θ is the contact angle that the ice−water interface makes with the confining pore wall as measured through the liquid water and *d* is the dendrite width at the base of tip protuberance.

2.4 Statistical analysis

All experimental data was shown as mean ± σ^2, as a result of, at least, triplicate experiments, for N=94 total dendrites analyzed. Statistical significance was assessed with an ordinary ANOVA, with *p*-value significance being reported as threshold values of 0.12 (ns), 0.033 (*), 0.002 (**) and <0.001 (***), for a 95% confidence interval (α=0.05).

3. Results

3.2 Interfacial ice patterns

FucoPol, a cryoprotective bio-based polysaccharide, was probed for its ice modulating capabilities, and compared with a small sugar molecule, sucrose, in a directional freezing setting.

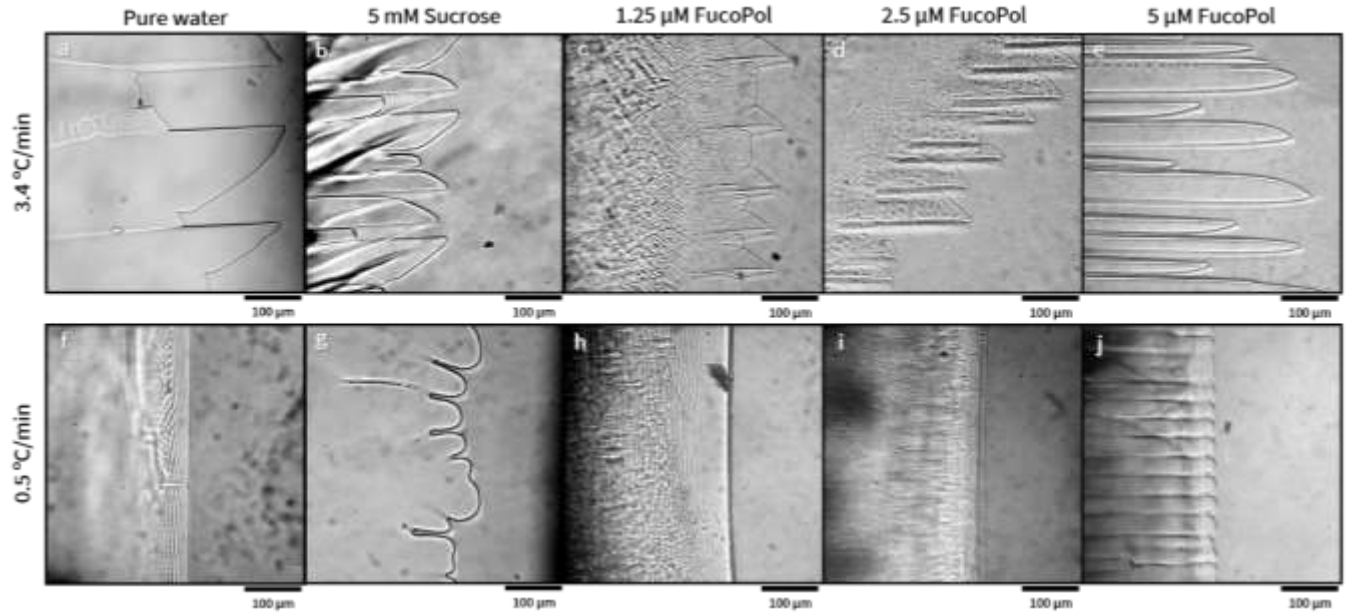

Figure 3. Photomicrographs of directionally frozen aqueous solutions at constrasting cooling rates, 3.4 and 0.5 °C/min. The conditions tested were pure water (***a***,***f***), 5 mM sucrose (***b***,***g***), 1.25 (***c***,***h***), 2.5 (***d***,***i***) and 5 µM FucoPol (***e***,***j***). The ice front is static from the image acquisition frame of reference, although a moving thermal gradient generates dendrite growth. Image magnification: 100×.

Table 1. Summary of qualitative analysis of photomicrographs for different directional freezing conditions. The scale is a relative perception score (1-3) of the observed trait.

Sample	Cooling rate	Granularity	Orthogonal striation	Lamellar stacking	Side branching
Water	3.4 °C/min	*	*	**	*
1.25 µM FucoPol		***	*	***	***
2.5 µM FucoPol		***	*	**	**
5 µM FucoPol		*	*	*	*
5 mM Sucrose		*	*	***	*
Water	0.5 °C/min	*	***	*	*
1.25 µM FucoPol		***	***	***	**
2.5 µM FucoPol		***	**	***	**
5 µM FucoPol		*	*	**	*
5 mM Sucrose		*	*	*	*

Figure 3 shows the dendritic appearance of ice crystals under the influence of different solute types and concentrations, at two different cooling rates. **Table 1** qualitatively describes the characteristics of each interfacial pattern. Pure water froze unidirectionally to form single-layered, transparent, conjoined dendrites that assumed an asymmetrical obloid shape, where its tip is sharp and anisotropically displaced from the center axis of growth, the *Z*-axis (**Figure 3*a***). Sucrose generated an anisotropic perturbation of the ice front on both the arbitrary *Z*-axis of directional growth and the orthogonal *y*-axis, in the sense that ice dendrites show dense, disorganized, lamellar stacking (**Figure 3*b***). Contrary to sucrose, the cumulative addition of FucoPol (**Figures 3*c*–*e***) results in the progressive isotropic alignment of dendrites accompanied by a shapeshifting from obloid to spicular morphology that is congruent with an increase in polysaccharide concentration. At 5 µM FucoPol, greater tip symmetry, enhanced interdendritic alignment and reduced width are observed (**Figure 3*e***). Dendritic granularity and side branching also progressively decreased with FucoPol concentration (**Table 1**). At lower concentrations of solute, there are perturbations in the solid bulk that result in a granular appearance, but such was not observed for 5 µM FucoPol. The dynamic nature of dendritic formation implies a phase change and solute supersaturation due to a reduction in the unfrozen water fraction, leading to an increase in viscosity and reduced diffusivity. Thus, it implies that polymer-polymer interactions eventually become predominant over polymer-water interactions, which agrees with the known entanglement regime for FucoPol at this concentration[34]. The temporal evolution of viscosity may also explain the gradual fadeout of dendrite texture from granular to smooth, as dendrites continued to grow in the presence of FucoPol. Lamellar stacking was observed for almost all conditions containing a molecular additive, although sucrose contains several cross-intersecting dendrites. The only exception was 5 µM FucoPol, which was able to preserve the single-layer characteristic of pure ice dendrites, but with significantly decreased thickness and

improved *Z*-alignment (**Figure 3*e***) when compared to sucrose (**Figure 3*b***). Ultimately, FucoPol showed a significant ice modulating effect at the water-ice interface. The emergence of increased primary spacing and brine channels between dendrites (**Figure 3*e***) leading to segregated spicular structures arises from a strong binding of the polysaccharide to kink sites that preclude the stepwise advancement of the ice front. Kink site development is more noticeable at slower cooling rates (**Figure 3*j***) and led to blunt tubular shapes rather than sharp spicules.

3.3 Effect of solute type and concentration

To descriptively assess the effects of each solute and concentration on ice dendrites, we performed a quantitative geometric parameter analysis of dendritic morphology for *N*=94 dendrites obtained in seven experimental triplicate runs. The results are shown in **Figure 4** and summarized in **Table 2**. For each test condition, parameters like lamellar thickness, tip protuberance, tip growth anisotropy, tilt angle, sharpness coefficient and primary spacing between neighboring dendrites were determined. The geometric definitions are described in **Figure 4*a***. Under a –3.4 ℃/min cooling rate, ice dendrites in the presence of 5 mM sucrose are 27% narrower than pure ice dendrites (**Figure 4*b***), 2.1-fold more protruded (**Figure 4*c***), 3.6-fold sharper (**Table 2**), have a similar tilt angle to pure water (**Figure 4*e***) and reduced tip anisotropy (**Figure 4*f***), *i.e.* generating a more centered tip. Primary spacing was also reduced by 42%, but still remained higher than all FucoPol conditions (**Figure 4*d***) and exclusively showed from extensive lamellar stacking, which led to overtly disorganized *Z*-growth (**Figure 3*b***) or side branching leakage in some runs. With FucoPol, lamellar thickness was significantly reduced from a maximum 92 μm (pure ice) to a minimum 19.8 μm (2.5 µM FP). Primary spacing between dendritic tips was objectively smaller under the presence of both solutes (**Figure 4*d***), with the emergence of brine channel depth for higher solute concentrations (**Figure 3*e***). The latter resulted in enhanced concavity and depth of the interdendritic spacings (**Figure 3*e***), generating spicules at an extreme and suggesting the strong affinity of the polysaccharide for specific kink sites in the ice front. The rather unvariant average primary spacing value between low and high FucoPol solutions (*ca.* 22–30 µm) (**Table 2**) and its distinction from sucrose (*ca.* 40–46 µm) and pure water averages (*ca.* 110 µm) also suggests a characteristic preferential spacing between FucoPol molecules binding to the kinks of the ice front. The addition of increasing concentrations of FucoPol promotes an overall dendritic alignment along the *Z*-axis of directional growth, with the tilt angle reducing from *ca.* 2.5^{o} for pure water down to *ca.* 1.4^{o} (**Figure 4*e***). Although no significant changes in tilt angle are noted, the absence of lamellar stacking in comparison to sucrose is significant. Tip protuberance (**Figure 4*c***) however, reduced from 90.4 to 47.7 μm for 1.25 µM FucoPol and 19.8 μm for 2.5 µM FucoPol. At 5 µM, the basal ice front was absent, replaced by continuous brine channels. Pure ice dendrites have a *Z*-growth anisotropy ratio of 0.71, which decreases to 0.4 in the presence of 5 µM FucoPol, indicating more isotropic tip growth.

Essentially, increasing FucoPol concentration consistently generates a progressive alignment and centering of the dendritic tip, contributing to uniform, closely packed, isotropic *Z*-growth, contrary to what was observed for sucrose. As for FucoPol concentration, different values provide shape tunability due to proportionally different viscosity values, exerting different magnitudes of a modulatory effect on the ice front. Increased viscosity also explains forced alignment as it constrains diffusional degrees of freedom from water molecules constituting the dendrite. The reduction in tip sharpness coefficient (**Table 2**) from 0.51 (*blunt*) for pure water down to 0.14 (*sharp*) for 5 µM FucoPol might arise from the Gibbs-Thomson effect. As concentration increases, dendrites transition from broad obloid shapes (pure water), through progressively rhombohedral dendrites (1.25, 2.5 µM FucoPol), to a spicular shape (5 µM FucoPol). From an interfacial energetics standpoint, sharp surfaces have a higher interfacial energy, hindering further water molecule migration towards tip growth, reflecting a growth inhibition effect due to adsorption.

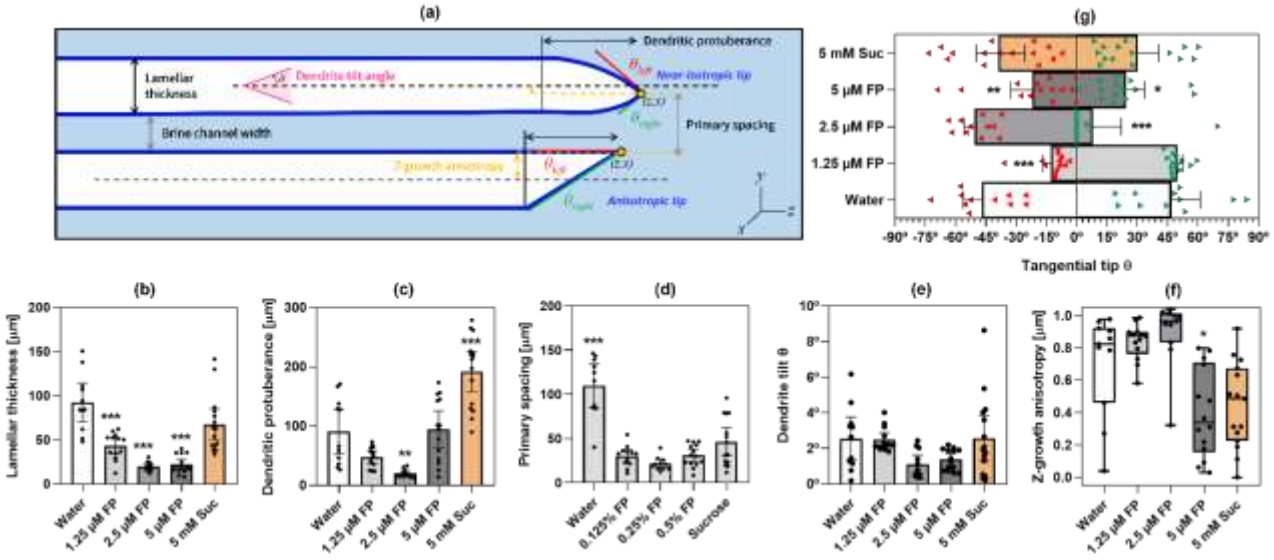

Figure 4. Summary of descriptive features of directionally frozen dendrites under a 3.4 ℃/min cooling rate in pure water (white) or in the presence of 1.25, 2.5, 5 µM FucoPol (*FP*, grey) and 5 mM sucrose (*Suc*, brown). Lengths are shown in μm. Error bars correspond to 95% CI. Data was collected from at least N=10 dendrites for each condition, obtained from triplicate experiments. Statistical significance identifiers (* $p \leq 0.03$, ** $p \leq 0.002$, *** $p \leq 0.001$) correspond to a hypothesis testing of different solutes exerting a difference in each dendritic parameter, compared to pure water.

Table 2. Summary of quantitative analysis of photomicrographs for different directional freezing conditions. Lengths are in μm.

Sample	Cooling rate	Lamellar thickness	Dendritic tip protuberance	Dendrite tilt angle	Tip sharpness coefficient	*Z*-growth anisotropy	Primary spacing	N
Water	3.4 ℃/min	92.0±32.8	90.4±56.3	2.56±1.80	0.51±0.16	0.71±0.31	109.7±34.4	11
1.25 µM FucoPol	3.4 ℃/min	42.9±14.9	47.7±17.3	2.47±0.67	0.29±0.03	0.84±0.11	30.2±11.9	13
2.5 µM FucoPol	3.4 ℃/min	19.8±5.2	19.8±7.0	1.12±0.77	0.01±0.005	0.90±0.21	21.6±7.4	11
5 µM FucoPol	3.4 ℃/min	21.9±10.4	94.7±53.5	1.36±0.60	0.14±0.09	0.40±0.27	31.1±12.5	14
	0.5 ℃/min	17.3±4.4	8.5±2.7	0.87±0.61	0.006±0.004	0.12±0.11	22.4±4.0	20
5 mM Sucrose	3.4 ℃/min	67.2±32.5	191.7±59.9	2.57±2.29	0.18±0.11	0.44±0.27	46.33±27.6	15
	0.5 ℃/min	39.7±14.9	41.9±14.6	17.0±13.7	0.40±0.11	0.24±0.17	41.7±14.7	10

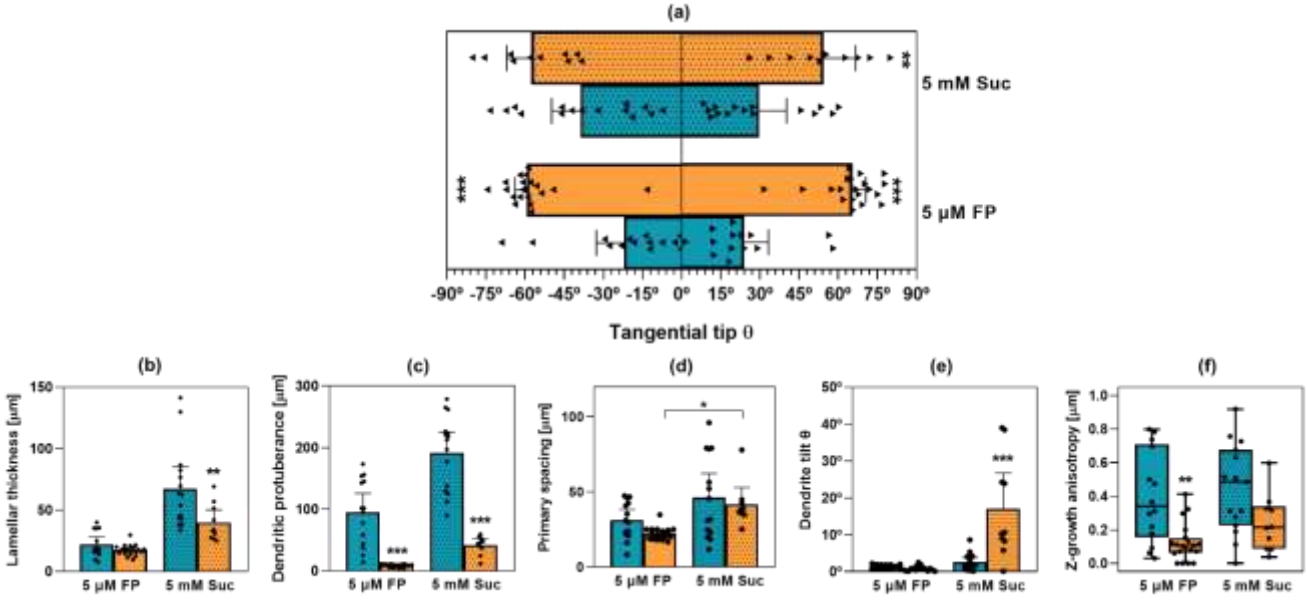

Figure 5. Effect of cooling rate on the dendritic features of directionally frozen 5 µM FucoPol and 5 mM sucrose samples (*a–f*) and resulting contact angle determination for dendrites grown in 5 µM FucoPol (*g*). Blue and orange correspond to cooling rates of 3.4 °C/min and 0.5 °C/min, respectively. Lengths are shown in μm. Error bars correspond to 95% CI. Data was collected from at least N=10 dendrites for each condition, obtained from triplicate experiments. Statistical significance identifiers (* $p \leq 0.03$, ** $p \leq 0.002$, *** $p \leq 0.001$) correspond to a hypothesis testing of different cooling rates exerting a difference in each dendritic parameter, for each sample. Panel (g) is a zoom-in of Figure 2*j*, representing schematically the determination of the polysaccharide-ice-water contact angle ϑ, rationalized as a cylindrical pore-confined geometry. Dendrite width *d* at the base of tip protuberance and dendrite number (*1–6*) for which ϑ was determined is also shown.

3.4 Effect of cooling rate

The cooling rate applied can be modulated by the pulling velocity under a constant thermal gradient. As it is proportional to interfacial velocity, it generates a distinct dendritic pattern. **Figure 5** shows the observed dendritic parameter differences between 5 mM sucrose and 5 µM FucoPol samples, under cooling rates of –3.4 °C/min (blue) and –0.5 °C/min (orange). A slower applied cooling rate (–0.5 °C/min) is conducive to lower dendritic lamellar thickness (**Figure 5*b***), tip protuberance (**Figure 5*c***) and *Z*-growth anisotropy (**Figure 5*f***) for both sucrose and FucoPol solutions. Lamellar thickness dropped from average 67.2 to 39.7 μm for sucrose and 21.9 to 17.3 μm for FucoPol; tip protuberance was reduced from 191.7 to 41.9 μm for sucrose and 94.7 to 8.5 μm for FucoPol; and *Z*-growth anisotropy decreased from 0.44 to 0.24 for sucrose and 0.40 to 0.12 for FucoPol. Essentially, a slower cooling rate generated ice front progression in a steadier, more stepwise fashion, whereas dendrites have smaller widths with blunt, centered, less-protruded tips. This is in agreement with reduced side branching but increased orthogonal striation (**Table 1**). The slower growth of an ice front corrects potential side branching, leading to greater dendrite symmetry (**Figures 3*a,f***), but results in increased orthogonal striation, as the stepwise advancement of the solid phase is more pronounced (**Table 1**). It is particularly noticeable in **Figures 3*e,j*** that dendritic alignment is significantly better in the presence of 5 µM FucoPol than any other condition, with better discrete separation of dendrites.

In what concerns tilt angle, tip sharpness coefficient and primary spacing, the trend is sample-specific. At –0.5 °C/min, a 5 µM FucoPol sample had a slightly decreased tilt angle compared to faster cooling and great alignment, while sucrose still preserved the characteristic degree of misalignment relative to the *Z*-axis. Tip sharpness reduced from 0.14 to 0.006 with 5 µM FucoPol, creating highly symmetrical, semi-spherical dendrite tips in the advancing ice front, while for sucrose, an increase from 0.18 to 0.40 was observed. Lastly, primary spacing reduced from 31.1 to 22.4 μm with 5 µM FucoPol, generating better dendrite packing, while for sucrose only a 10% reduction in primary spacing was observed, although lamellar superposition was eliminated.

Ultimately, a slower cooling rate emphasized the ice-binding interactions of each sample type. For sucrose, slower cooling eliminated dense lamellar stacking at the expense of worse dendritic alignment, robustness and separation. For 5 µM FucoPol, the very thin, highly aligned appearance of dendrites was preserved, alongside an increase in tight junction packing, resulting in a more uniform front. In the context of applicability, if a highly symmetrical tubular structure is the desired interfacial pattern, the usage of high molecular weight FucoPol is preferred over sucrose due to its modulatory effect and ability to finetune dendrite width, length, packing and sharpness, the latter tunable by the cooling rate applied.

3.5 Contact angle

The ice modulatory effect of FucoPol hinted at a polysaccharide-ice binding effect that is usually reflected in surface modifications, such as the contact angle between the solid and liquid phases. Thus, the polysaccharide-ice-water contact angle θ was determined for the interfacial pattern obtained with a 5

µM FucoPol solution at –0.5 ℃/min, made simple by its uniform growth (**Figure 5*g***). Here we adopted a cylindrical pore-confined geometrical approximation of the growth space, which has been used before in determining the protein-ice-water contact angle[39], as antifreeze proteins modulate ice in the same fashion[40]. This approximation assumes that a dendrite growing in the *z*-axis is confined by chemical barriers of ice modulator (in this case, FP) that extend parallel to its growth (**Figure 5*g*,** blue lines), imposing an interface curvature. The previous observation of extensive interdendritic depth (**Figure 3*e***) suggested that the binding of FucoPol to a kink site hinders further ice growth in the space it occupies, rendering this approximation valid for the determination of θ. From Eq. 1, we have computed that an initial FucoPol concentration of 5 µM results in an average dendrite tip width *d* of 11.8±0.6 μm and a polysaccharide-ice contact angle θ of 52.6±2.2º. Surface curvature was consistently symmetric, varying just by 1º for left (53.5±2.0º) and right (51.8±2.0º) θ values.

3.6 Thermal hysteresis

The imposing of an interface curvature by FucoPol also implies that a freezing point change ensues[41], due to a change in surface energetics. Thermal hysteresis (TH), a common property observed in cryoprotectants and antifreeze proteins where the kinetic freezing point deviates from the equilibrium freezing point (otherwise known as the melting point) was determined from contact angle determinations. From the Gibbs-Thomson equation (Eq. 1), and assuming a uniform density of FucoPol molecules along the surface curvature of a dendrite, an average absolute TH of 6.7±1.6 ℃ was obtained for ice curvature induced by 5 µM FucoPol. Depending on each individual dendrite, TH varied between 3.4 and 8.1 ℃. This value is in agreement with previous thermal hysteresis data collected from differential scanning calorimetry experiments using FucoPol[8], where the average kinetic freezing points for pure water and 0.5–1% FucoPol solutions were –19.2±0.5 ℃ and –14.1±1 ℃, respectively, yielding a TH interval of 3.6–6.6 ℃.

4. Discussion

The transition from obloid-shaped, anisotropically grown, broad, sharp, misaligned ice dendrites to tubular-shaped, isotropic, symmetric, blunt, *Z*-aligned dendrites is of great interest in cryopreservation. Directional freezing has shown benefits in cryobiology[18,19], as controlling ice growth directionality has been highlighted as the best strategy for biological preservation in cells[20], tissues and organs[21]. Now, the modulation of instabilities during dendritic development towards beneficial shapes by the addition of a solute of interest becomes a new approach towards tackling the ice growth problem. The resulting dendritic appearance depends not only on the type of solute used, but a myriad of experimental conditions, such as cooling rate, interfacial velocity, solution diffusivity and molality, which are transversal parameters to both directional freezing and conventional cryopreservation procedures.

FucoPol, a bio-based fucose-rich polysaccharide, has shown a significant ice modulatory effect at the water-ice interface, adding to the collective understanding of its cryoprotective effect. The effect appears dose-independent, as the highest molar FucoPol concentration (5 μM) generated a significantly different outcome from 5 mM sucrose. This inference aligns with its non-colligative nature observed before[8]. The two most prominent features of FucoPol usage were (i) dendritic alignment and (ii) shape tunability. First, the proper alignment of dendritic growth with the thermal gradient is beneficial in directional freezing because such experimental control aligns with the desired outcome: creating highly symmetrical dendrites without disorganized lamellar stacking. Unlike sucrose, side branching leakage was not observed for FucoPol solutions, which leverage an increased solution viscosity towards generating a uniform ice front where orthogonal diffusivity of water molecules is hindered. Slow cooling with 5 μM FucoPol resulted in extensively better overall dendrite alignment than with 5 mM sucrose, although their individual tilt angles varied. This is a consequence of the initial conditions of ice growth, hereby promoted by multidirectional nucleation, which regulate and determine the degree of uncertain in angle orientation. Thus, although *Z*-alignment may be interpreted in a broader sense, careful considerations should be taken when scrutinizing tilt angles as a sole consequence of solute influence.

Second, the strong ice modulatory effect of FucoPol can be finetuned by the cooling rate applied, generating spicular (–3.4 ℃/min) or tubular (–0.5 ℃/min) dendrites, both of high symmetry and alignment, the only major reshaping being the sharpness of the dendrite. The sharp surfaces of spicular dendrites have a higher interfacial energy than those of pure water, which may lead to hindering water molecule migration towards tip growth, resolving into ice growth inhibition. Zhang *et al.*[42] showed that PVA, the most potent ice recrystallization inhibiting (IRI) biomimetic polymer right after antifreeze glycoproteins[43], could only develop kinetic V-shaped dendrites (past the adsorption-controlled planar ice front) at concentrations 5–10 wt. %, which attests to the powerful effect of FucoPol at 0.5 wt.%.

Regardless of the cooling rate, the significant interdendritic depth (brine channels) obtained at –3.4 ℃/min (**Figure 3*e***) or the nuanced emergence of preclusive kink sites in the ice front at –0.5 ℃/min (**Figure 3*j***) point to the same mechanism of action: a Gibbs-Thomson binding effect. The modulatory action of type I antifreeze proteins[35] and rattlesnake venom lectins[27] in ice front progression was morphologically similar to FucoPol. These molecules are known to act by an adsorption-inhibition mechanism, in which they preclude the access of water molecules to a growing ice lattice by binding to the ice front, exerting a local ice curvature separated by kink sites and exerting kinetic inhibition[40]. FucoPol (5 mg/ml, 2–3.5 MDa) also behaved similarly to thermal hysteresis proteins (THP, 5–15 mg/ml, 3–30 kDa)[44].

The strong modulation of the interfacial pattern, alongside a determined polysaccharide-ice-water contact angle of 52.6±2.2º, also corroborates an active Gibbs-Thomson binding effect of the polysaccharide chain to the specific binding surface

of the ice front. For reference, 10% DMSO[45] only generated a perturbation of θ=12º, while the hyperactive antifreeze protein from *Tenebrio molitor*[39] resulted in θ=87.5º. A 5 μM FucoPol solution induced a (relatively) moderate surface curvature similar to an ice-phobic substrate[46], composed of sequentially linked APTMS, glutaraldehyde and an antifreeze polypeptide (θ=59.6±0.9º), revealing some extent of water structuring[39]. It is expected that the potent ice modulatory effect of FucoPol should not outperform an antifreeze protein, as the periodic binding sequences and smaller molecular lengths observed for naturally selected antifreeze proteins most likely contribute to maximizing binding affinity to a greater extent than the structural repeating units of a large anionic polysaccharide that undergoes chain entanglement. Thus, under such incidental conditions, the modulatory effect of FucoPol is still remarkable.

A significant change in contact angle is accompanied by a change in surface energetics, which reflects a change in the local kinetic freezing point. This concept was proposed by Drori, Davies and Braslavsky[41], who interpreted thermal hysteresis as being curvature-induced, whereas ice was only allowed to grow in regions absent of antifreeze protein or in regions where the antifreeze protein is adsorbed through non-ice binding domains. An average absolute TH of 6.7±1.6 ℃ was obtained for ice curvature induced by 5 μM FucoPol. It is interesting to observe an agreeably similar TH interval for both directional freezing and DSC[8] experiments, considering their dissimilar nature; one involving dynamic unidirectional growth of dendrites, the other a static isotropic freezing of a droplet.

We further attempted to pinpoint the nature of concentration-dependent observations for FucoPol interfacial patterns. The dynamic nature of directional freezing implies that, during dendritic growth, a decrease in the unfrozen fraction generates a progressive solute supersaturation that maximizes liquid-phase viscosity and minimizes molecular diffusivity. In a length-scale, it creates a solutal diffusion field. Nagashima *et al.*[47] showed that dendritic instabilities respond to such a concentration gradient and ice shaping is maximized by a transiently higher concentration at the interface. Moreover, locally different compositions can create visually retreating layers of dendrites due to melting point depression. Zhang et al.[48] corroborated these findings and added that a solutal diffusion field depends on solute type, such that a diffusive flow will promote side branching in a more appreciable way than residual orthogonal thermal fluxes[49] due to a greater contribution towards phase heterogeneity. In colloidal suspensions especially, the tip would appear ragged and retreated on one side (solute-rich) and smooth on another (water-rich)[48]. This was observed for starting lower concentrations of FucoPol but not 5 μM, suggesting that while in the former there is appreciable diffusive flow, the latter behaves as viscous and effectively suppresses side branching leakage, hence the observed ice front uniformity. A pulling velocity 7-fold slower further exacerbated this behavior. Three observations sustain the validity of increased viscosity towards explaining the high uniformity of the ice front: (i) a visual retreat of dendrites growing on top of developed ones in the bottom layer can be observed in **Figure 3*j***, which agrees with Nagashima *et al.*[47], (ii) the anisotropic tip raggedness characteristic of diffusive flow fades to smooth symmetrical dendrites at higher FucoPol concentrations, which agrees with Zhang et al.[48], and (iii) Torres et al.[34] has determined that a 0.5 wt.% (5 μM) FucoPol concentration lies in a high entanglement regime that potentiates polymer-polymer interactions and generates higher intrinsic viscosity. Ultimately, the ice modulatory effect of FucoPol relies on two fundamental aspects: a Gibbs-Thomson effect induced by the chemical nature of the polysaccharide, with its binding and non-binding regions; and a viscosity-dependent modulation of the liquid dynamics at the interface. At 5 μM FucoPol, a greater number of binding regions and increased viscosity have a growth inhibitory effect, establishing kink sites whilst hindering molecular mobility.

FucoPol-mediated ice modulation in directional freezing further contributed towards explaining its comprehensive cryoprotective action[8–10], but its versatility of use for dendrite reshaping is suggestive of future impact in tissue engineering. 3D bioprinting has leveraged directional freezing to design microscopic structures for biological applications, coined as 3D cryobioprinting[38]. Directional ice growth inside an alginate matrix induced scaffold structuration that can be retained post-thaw[50], and has since been optimized to successfully preserve a 10-layer matrix of live cells[51]. Other polymer strategies combine ice-etching scaffolds with chemical crosslinking or density-gradient cell migration[52–54], but the ice reshaping ability of biocompatible, biodegradable FucoPol (along with its verified 3D-printability (*Figure SI.2*)) quickly enables the ice-etching of a matrix without using reagents that are toxic or require washout. In particular, the tightly packed, uniform, tubular dendrites formed with FucoPol can be used to design microvascular channels, generating model substrates for extensive biochemical research.

5. Conclusions

FucoPol, a fucose-rich bio-based polysaccharide, has demonstrated beneficial ice modulatory effects that align with its cryoprotective function. A directionally frozen 5 μM FucoPol aqueous solution is able to deliver symmetric, *Z*-aligned ice dendrites with tunable sharpness under variable cooling rate. The modulatory effect of FucoPol differs from that of sucrose both in desired outcome, quality of outcome and mechanism of action, showing a non-colligative Gibbs-Thomson ~~binding~~ effect alluding to ~~that~~ the adsorption-inhibition mechanism of antifreeze proteins, most resembling the ice modulatory effects of the type I antifreeze protein and rattlesnake venom lectin, at a molality three orders of magnitude lower than sucrose. FucoPol shows promising intentional design potential in 3D cryobioprinting, able to generate thin tubules of 17.3±4.4 μm in width (5.3-fold reduction from pure water), tightly packed with neighboring dendrites (22.4±4.0 μm primary spacing, without lamellar stacking), aligned with the thermal gradient (0.87±0.61º tilt angle, 3-fold enhanced directionality control), with dendritic tips 5.9-fold more symmetric. Depending on the cooling rate applied, tip morphology can range from sharp spicules (0.14±0.09 sharpness coefficient, 3.6-fold less sharp

than pure water) to blunt tubules (0.006±0.004). Ultimately, the ice modulatory effect of 5 µM FucoPol, along with an ice front stabilizing effect of viscosity due to polymer entanglement, shows promise in tissue engineering applications that leverage ice-etching using biodegradable, non-toxic reagents with ease of removal for designing biomimetic scaffolds.

Author Contributions

B.M.G. conceptualized study, performed experiments, data analysis, and wrote manuscript. **L.T.L.** conceptualized study, performed experiments and reviewed manuscript. **B.R.** conceptualized study, reviewed manuscript, provided resources, and supervised. **F.F.** provided resources, reviewed manuscript, and supervised. All authors have read and agreed to the published version of the manuscript.

Conflicts of interest

There are no conflicts to declare.

Acknowledgements

This work received financial support from the National Science Foundation (NSF) Graduate Research Fellowship under Grant No. DGE 1752814, the NSF Engineering Research Center for Advanced Technologies for Preservation of Biological Systems (ATP-Bio) under NSF EEC Grant No. 1941543 and national funds from FCT - Fundação para a Ciência e a Tecnologia, I.P. (Portugal), in the scope of projects UIDP/04378/2020 and UIDB/04378/2020 of the Research Unit on Applied Molecular Biosciences—UCIBIO and LA/P/0140/2020 of the Associate Laboratory Institute for Health and Bioeconomy—i4HB. B. M. Guerreiro also acknowledges PhD grant funding by Fundação para a Ciência e a Tecnologia, FCT I.P. (SFRH/BD/144258/2019) and supporting personal funding from Fulbright Portugal (21-066), Fundação Luso-Americana para o Desenvolvimento, FLAD (Proj. 2021/0070 – G-2021-0052) and The Company of Biologists (JCSTF2105556). The authors would like to thank L. Warburton for valuable insights on cryobioprinting and tissue engineering.

References

1 D. E. Pegg, *Cryobiology*, 2010, **60**, S36–S44.
2 K. A. Murray and M. I. Gibson, *Nat. Rev. Chem. 2022 68*, 2022, **6**, 579–593.
3 C. I. Biggs, T. L. Bailey, Ben Graham, C. Stubbs, A. Fayter and M. I. Gibson, *Nat. Commun. 2017 81*, 2017, **8**, 1–12.
4 Y. Yeh and R. E. Feeney, *Chem. Rev.*, 1996, **96**, 601–618.
5 C. Stubbs, J. Lipecki and M. I. Gibson, *Biomacromolecules*, 2017, **18**, 295–302.
6 K. Matsumura and S. H. Hyon, *Biomaterials*, 2009, **30**, 4842–4849.
7 D. E. Mitchell, N. R. Cameron and M. I. Gibson, *Chem. Commun.*, 2015, **51**, 12977–12980.
8 B. M. Guerreiro, F. Freitas, J. C. Lima, J. C. Silva, M. Dionísio and M. A. M. Reis, *Carbohydr. Polym.*, 2020, **245**, 116500.
9 B. M. Guerreiro, J. C. Silva, C. A. V. Torres, V. D. Alves, J. C. Lima, M. A. M. Reis and F. Freitas, *ACS Appl. Bio Mater.*, 2021, **4**, 4800–4808.
10 B. M. Guerreiro, A. N. Consiglio, B. Rubinsky, M. J. Powell-Palm and F. Freitas, *ACS Biomater. Sci. Eng.*, 2022, **2022**, 1852–1859.
11 S. Carillo, A. Casillo, G. Pieretti, E. Parrilli, F. Sannino, M. Bayer-Giraldi, S. Cosconati, E. Novellino, M. Ewert, J. W. Deming, R. Lanzetta, G. Marino, M. Parrilli, A. Randazzo, M. L. Tutino and M. M. Corsaro, *J. Am. Chem. Soc.*, 2015, **137**, 179–189.
12 G. M. Fahy and B. Wowk, *Methods Mol. Biol.*, 2015, **1257**, 21–82.
13 G. D. Elliott, S. Wang and B. J. Fuller, *Cryobiology*, 2017, **76**, 74–91.
14 B. Rubinsky and M. Ikeda, *Cryobiology*, 1985, **22**, 55–68.
15 B. Rubinsky, *J. Cryst. Growth*, 1983, **62**, 513–522.
16 H. L. Tsai and B. Rubinsky, *J. Cryst. Growth*, 1984, **70**, 56–63.
17 M. Gündüz and E. Çadirli, *Mater. Sci. Eng. A*, 2002, **327**, 167–185.
18 A. Arav and J. Saragusty, *Reprod. Fertil. Dev.*, 2013, **26**, 83–90.
19 A. Arav, B. Rubinsky, G. Fletcher and E. Seren, *Mol. Reprod. Dev.*, 1993, **36**, 488–493.
20 L. Bahari, A. Bein, V. Yashunsky and I. Braslavsky, *PLoS One*, 2018, **13**, e0192265.
21 A. Arav, *Cells 2022, Vol. 11, Page 1072*, 2022, **11**, 1072.
22 W. Kurz, D.J. Fisher, *Fundamentals of solidification,* Trans Tech Publications, 1998.
23 G. Kopstad and A. Elgsaeter, *Biophys. J.*, 1982, **40**, 155–161.
24 B. Rubinsky, *Exp. Heat Transf.*, 2007, **10**, 1–29.
25 H. Ishiguro and B. Rubinsky, *Cryobiology*, 1994, **31**, 483–500.
26 K. V. Ewart, B. Rubinsky and G. L. Fletcher, *Biochem. Biophys. Res. Commun.*, 1992, **185**, 335–340.
27 B. Rubinsky, R. Coger, K. V. Ewart and G. L. Fletcher, *Nat.* 1992, **360**, 113–114.
28 H. Ishiguro and K. Koike, *Ann. N. Y. Acad. Sci.*, 1998, **858**, 235–244.
29 H. L. Tsai, B. Rubinsky, *J. Cryst. Growth*, 1984, **69**, 29–46.
30 J. A. Raymond and A. L. DeVries, *Proc. Natl. Acad. Sci. U. S. A.*, 1977, **74**, 2589–93.
31 L. Chapsky and B. Rubinsky, *FEBS Lett.*, 1997, **412**, 241–244.
32 F. Freitas, V. D. Alves, C. A. V. Torres, M. Cruz, I. Sousa, M. J. Melo, A. M. Ramos and M. A. M. Reis, *Carbohydr. Polym.*, 2011, **83**, 159–165.
33 H. Nada and Y. Furukawa, *Polym. J. 2012 447*, 2012, **44**, 690–698.
34 C. A. V. Torres, A. R. V. Ferreira, F. Freitas, M. A. M. Reis, I. Coelhoso, I. Sousa and V. D. Alves, *Int. J. Biol. Macromol.*, 2015, **79**, 611–617.
35 C. B. Marshall, A. Chakrabartty and P. L. Davies, *J. Biol. Chem.*, 2005, **280**, 17920–17929.

36 C. R. Shurer, J. C.-H. Kuo, L. M. Roberts, J. G. Gandhi, M. J. Colville, T. A. Enoki, H. Pan, J. Su, J. M. Noble, M. J. Hollander, J. P. O'Donnell, R. Yin, K. Pedram, L. Möckl, L. F. Kourkoutis, W. E. Moerner, C. R. Bertozzi, G. W. Feigenson, H. L. Reesink and M. J. Paszek, *Cell*, 2019, **177**, 1757-1770.e21.
37 A. R. V. Ferreira, C. A. V. Torres, F. Freitas, M. A. M. Reis, V. D. Alves and I. M. Coelhoso, *Int. J. Biol. Macromol.*, 2014, **71**, 111–116.
38 G. Ukpai and B. Rubinsky, *J. Heat Transfer*, 2020, **142**, 022401.
39 J. O. M. Karlsson, I. Braslavsky and J. A. W. Elliott, *Langmuir*, 2019, **35**, 7383–7387.
40 J. Barrett, *Int. J. Biochem. Cell Biol.*, 2001, **33**, 105–117.
41 R. Drori, P. L. Davies and I. Braslavsky, *RSC Adv.*, 2015, **5**, 7848–7853.
42 T. Zhang, L. Wang, Z. Wang, J. Li and J. Wang, *J. Phys. Chem. B*, 2021, **125**, 970–979.
43 P. M. Naullage and V. Molinero, *J. Am. Chem. Soc.*, 2020, **142**, 4356–4366.
44 R. Coger, B. Rubinsky and G. Fletcher, *J. Offshore Mech. Arct. Eng.*, 1994, **116**, 173–179.
45 S. Park, P. A. L. Wijethunga, H. Moon and B. Han, *Lab Chip*, 2011, **11**, 2212.
46 K. Koshio, K. Arai, T. Waku, P. W. Wilson and Y. Hagiwaraid, , *PLoS ONE,* 2018, **13**, e0204686.
47 K. Nagashima and Y. Furukawa, *J. Cryst. Growth*, 2000, **209**, 167–174.
48 T. Zhang, Z. Wang, L. Wang, J. Li and J. Wang, *Langmuir*, 2021, **37**, 10579–10587.
49 I. Braslavsky and S. G. Lipson, *J. Cryst. Growth*, 1999, **198**–**199**, 56–61.
50 L. Lou and B. Rubinsky, 2022, **144**, 1–7.
51 L. Warburton and B. Rubinsky, *Gels 2023,* **9***,* 502.
52 N. W. Meghri, A. E. Donius, B. W. Riblett, E. J. Martin, A. M. Clyne and U. G. K. Wegst, *JOM*, 2010, **62**, 71–75.
53 E. Hadjipanayi, V. Mudera and R. A. Brown, *Cell Motil. Cytoskeleton*, 2009, **66**, 121–128.
54 W. P. Daley, S. B. Peters and M. Larsen, *J. Cell Sci.*, 2008, **121**, 255–264.